Transport simulation and image reconstruction for fast-neutron detection of explosives and narcotics

Bradley J. Micklich, Charles L. Fink, and Leonid Sagalovsky

Technology Development Division, Argonne National Laboratory
Argonne, Illinois 60439 USA

ABSTRACT

Fast-neutron inspection techniques show considerable promise for explosive and narcotics detection. A key advantage of using fast neutrons is their sensitivity to low-Z elements (carbon, nitrogen, and oxygen), which are the primary constituents of these materials. We are currently investigating two interrogation methods in detail: Fast-Neutron Transmission Spectroscopy (FNTS) and Pulsed Fast-Neutron Analysis (PFNA). FNTS is being studied for explosives and narcotics detection in luggage and small containers for which the transmission ratio is greater than about 0.01. The Monte-Carlo radiation transport code MCNP is being used to simulate neutron transmission through a series of phantoms for a few (3-5) projection angles and modest (2 cm) resolution. Areal densities along projection rays are unfolded from the transmission data. Elemental abundances are obtained for individual voxels by tomographic reconstruction, and these reconstructed elemental images are combined to provide indications of the presence or absence of explosives or narcotics. PFNA techniques are being investigated for detection of narcotics in cargo containers because of the good penetration of the fast neutrons and the low attenuation of the resulting high-energy gamma-ray signatures. Analytic models and Monte-Carlo simulations are being used to explore the range of capabilities of PFNA techniques and to provide insight into systems engineering issues. Results of studies from both FNTS and PFNA techniques are presented.

1. INTRODUCTION

Fast-neutron interrogation techniques are being studied for the detection of illicit substances (e.g., explosives and drugs) in luggage and cargo containers. X-ray techniques are often unable to detect these substances. Fast-neutron based techniques are attractive because they offer the possibility of determining the densities of light elements such as carbon, nitrogen, and oxygen within individual volume elements. Explosives and narcotics are composed primarily of these elements, but have elemental densities and density ratios different from most other substances likely to be found in legitimate cargo. For example, explosives are relatively rich in oxygen and nitrogen but relatively poor in carbon, while narcotics are relatively poor in nitrogen and oxygen but relatively rich in carbon and hydrogen.

This paper discusses two different fast-neutron based techniques. The first technique, Fast-Neutron Transmission Spectroscopy (FNTS), is based on measuring the neutron spectrum from a distributed energy neutron source after the neutrons have passed through the items to be interrogated. The basic technique was first examined[1] for bulk material analysis, and is best suited for examination of luggage or small containers having an average transmission ratio greater than about 0.01. The second technique is based on detecting gamma rays from fast-neutron interactions with the material being interrogated. Volumetric elemental densities are determined by analyzing the characteristic gamma rays emitted from the material. We discuss the variant of the technique referred to as Pulsed Fast-Neutron Analysis (PFNA) being developed by Science Applications International Corporation.[2] This technique is suitable for examination of large containers because of the good penetration of the fast neutrons and the low attenuation of the high-energy gamma rays.

2. FAST-NEUTRON TRANSMISSION SPECTROSCOPY

Fast-Neutron Transmission Spectroscopy uses standard time-of-flight (TOF) techniques to measure the energy spectrum of neutrons emitted from a collimated continuum source before and after transmission through an interrogated sample. The transmission spectrum depends on the integrated density of the elements present in the line-of-sight from the neutron source to the detector and on the total cross sections of those elements. A schematic drawing of a typical FNTS system is shown in Figure 1. The collimator may define a pencil beam which obtains information about one projection line-of-sight (one pixel) at a time, or may define a fan beam which allows the interrogation of a line of pixels simultaneously if a linear detector array is used. The individual elemental areal densities are obtained by a linear least-squares unfolding of the transmission spectrum using the total cross sections for the elements of interest.[3]

DISCLAIMER

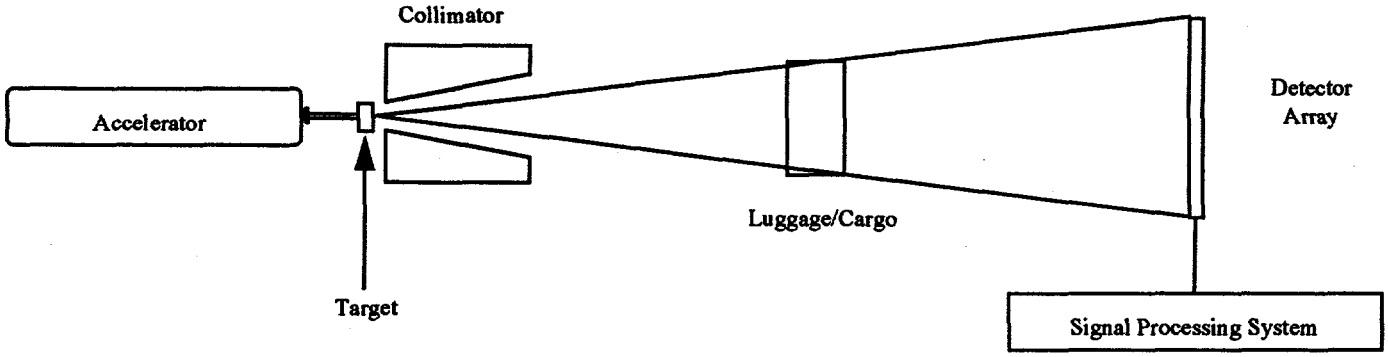

Figure 1. Schematic drawing of a Fast-Neutron Transmission Spectroscopy luggage/cargo inspection system.

2.1. Simulation and modeling

The Monte Carlo radiation transport code MCNP[4] was used to simulate neutron transmission through a number of luggage phantoms containing either bulk or sheet explosives or narcotics. The simulations assumed a parallel beam of neutrons irradiating a slice of the phantom, corresponding to a fan-beam geometry. The neutron source is the ^{9}Be(d,n) reaction at E_d = 5 MeV. This deuteron energy results in a source with high neutron yield in the range 1-4 MeV, which contains many resolved resonances for the light elements. The source-detector distance was 5 m, and the source and detector timing widths were 2 nsec. Analog transport was used (i.e., no variance reduction) so that each neutron from the source represents one neutron from a real source. The number of neutron histories run ($1.4 \cdot 10^6$ per pixel) was chosen to simulate a one-second exposure for a maximum count rate of 10^5/s in any given detector at an average transmission of 0.5. A simple three-body phantom containing a bulk explosive is shown in Figure 2(a). The transmission ratio as a function of neutron energy is shown in Figure 2(b) for a projection ray which passes from left to right through the two square objects. The transmission data are unfolded using a linear least-squares routine to determine the elemental areal densities, which are then fed into tomographic reconstruction routines (described below in Section 2.2).

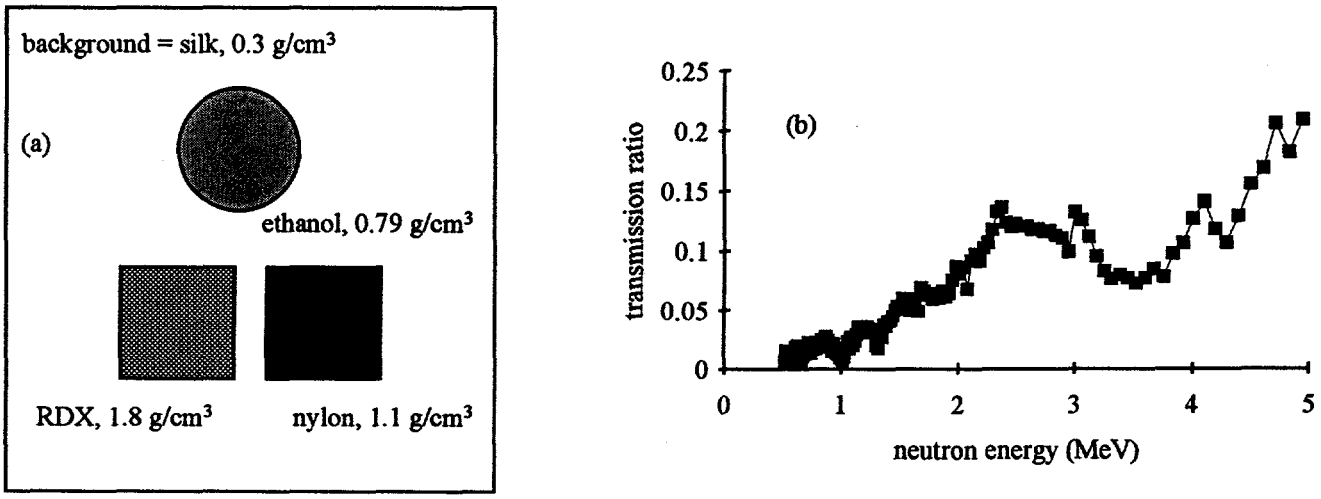

Figure 2. (a) Simple luggage phantom containing bulk objects. (b) Transmission ratio for projection ray which passes from left to right through the RDX and nylon square objects.

Several studies have been performed to understand how well the elemental areal densities can be determined, and what conditions lead to errors which are acceptable. In one set of simulations, transmission spectra were calculated for a variety of materials and material thicknesses. The errors in elemental density are shown in Figure 3 as functions of the transmission

ratio. In this figure the errors are normalized to the sample mean-free-path thickness, which is equivalent to expressing them as a percentage of the areal density. Several interesting features are apparent. First, the minimum errors are found for transmissions of about 0.13, which is what one would expect from theoretical considerations.[5] Second, not all elements have the same errors for a given transmission. Certain elements with distinctive features in the total cross section, such as oxygen, silicon, and carbon, have smaller errors than the others. Third, the error for a given element does not depend on whether the element is present in the sample (i.e., not all of the materials simulated contain all ten of the elements). This means that the errors are determined by counting statistics, the method used to perform the unfolding, and to some degree the cross sections themselves. Thus further studies on the behavior of errors (i.e., determining system parameters which lead to acceptable errors) need not be conducted with luggage phantoms or particular combinations of materials, but can be conducted with any material. We have generally chosen the high explosive RDX as the sample material for our studies.

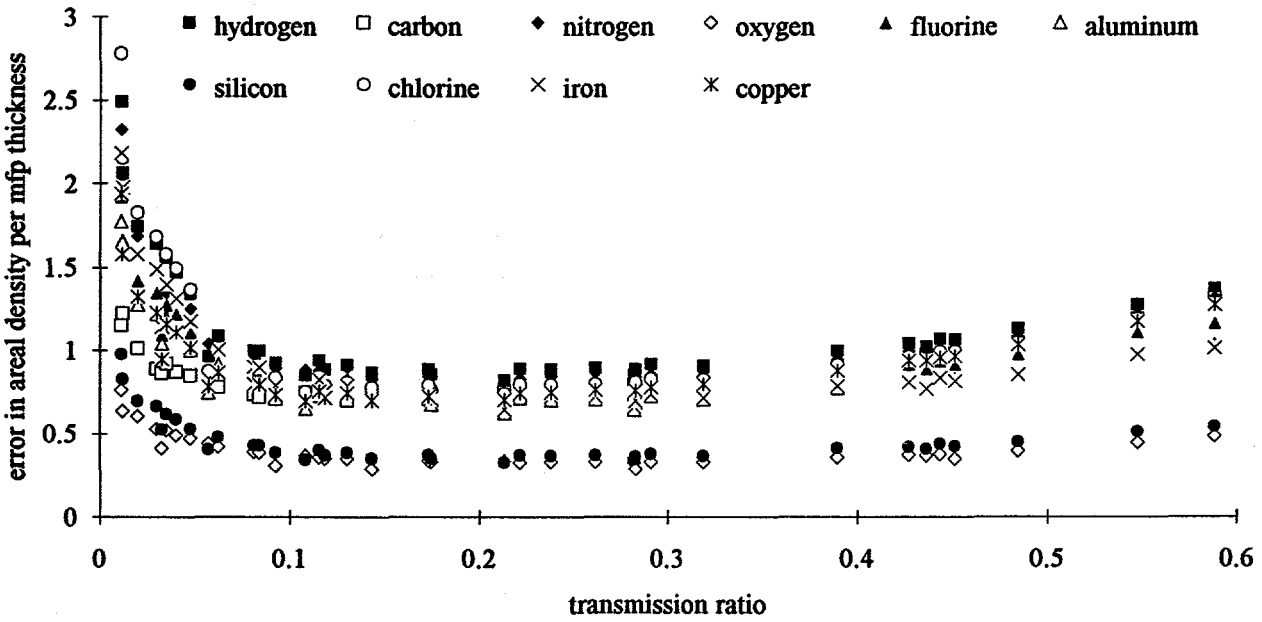

Figure 3. Error in unfolded areal density for ten elements used in the transmission unfolding algorithm, as a function of transmission ratio, for a variety of materials and material thicknesses. Simulation conditions were ^{9}Be(d,n) source with E_d = 5 MeV, 2 ns time bins, $1.4 \cdot 10^6$ neutron histories, and unfolding using the 0.5-10 MeV region of the neutron energy spectrum.

Also of interest is the behavior of the errors in areal density as functions of the number of neutron histories used in the simulations (i.e., irradiation time for a given accelerator current), the resolution of the time-of-flight system, and the energy range of the data considered by the unfolding algorithm. The errors in areal density for nitrogen and oxygen are shown in Figure 4 for several sets of conditions. For selected materials, simulations were run corresponding to two-second ($2.8 \cdot 10^6$ neutrons), one-second ($1.4 \cdot 10^6$ neutrons), one-half-second ($7 \cdot 10^5$ neutrons), and one-quarter second ($3.5 \cdot 10^5$ neutrons) irradiations, with all cases using the energy range of $0.5 \leq E_n \leq 10$ MeV for unfolding. The one-second-equivalent data were then analyzed using just the energy range $1 \leq E_n \leq 5$ MeV. These cutoffs were chosen because the neutron source and detector efficiency are small outside that range, yielding many fewer counts per time bin than for bins within that range. The resolution was decreased to 1 ns for the $1 \leq E_n \leq 5$ MeV data, which then gives about the same number of data points as using the energy range $0.5 \leq E_n \leq 10$ MeV at 2 ns resolution. The interesting results from these simulations are that (i) the curves for errors versus number of neutrons detected show a slope of -0.5 on a log-log plot, which is expected from statistics; (ii) the errors are increased only modestly when the smaller energy range is used, and (iii) using increased resolution over the smaller energy range has no effect on the errors. These results indicate that there is some useful information outside the energy range 1 to 5 MeV, but that ignoring it does not change the unfolded areal densities much, and that there is no benefit from reducing resolution beneath 2 ns. In fact, one could probably increase the time bin width somewhat, although decreased resolution could also be achieved by using a shorter flight path, which would also reduce the system's space requirement. Unfolding results for RDX and PETN for the simulations using $1.4 \cdot 10^6$ neutron histories are shown in Table 1.

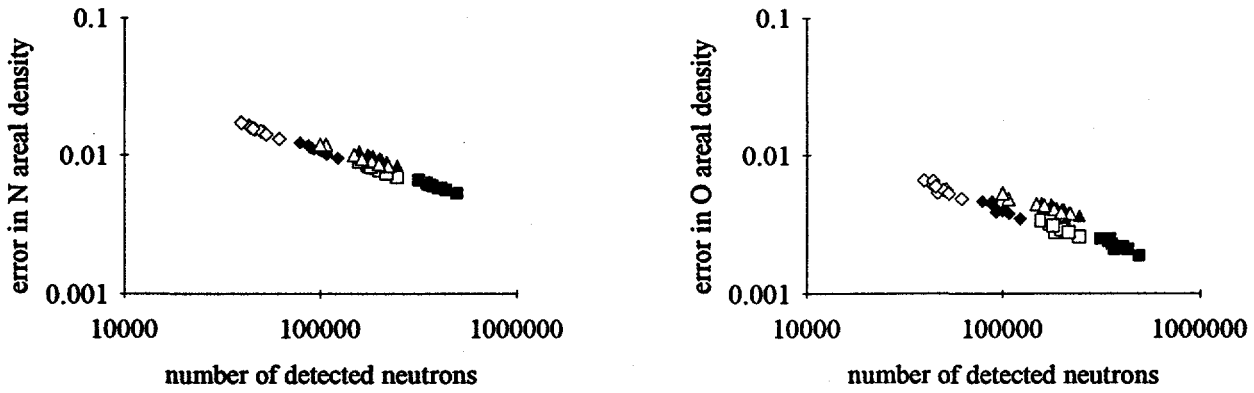

Figure 4. Variation in errors in unfolded elemental areal densities for nitrogen and oxygen for a variety of simulation conditions. The key to the symbols is (number of neutron histories, time bin width, energy range used in unfolding): ■: ($2.8 \cdot 10^6$, 2 ns, 0.5-10 MeV); □: ($1.4 \cdot 10^6$, 2 ns, 0.5-10 MeV); ♦: ($7 \cdot 10^5$, 2 ns, 0.5-10 MeV); ◊ : ($3.5 \cdot 10^5$, 2 ns, 0.5-10 MeV); ▲: ($1.4 \cdot 10^6$, 2 ns, 1-5 MeV); △: ($1.4 \cdot 10^6$, 1 ns, 1-5 MeV).

2.2. Development of contraband detection algorithms

The FNTS technique determines the elemental areal densities for objects located along the line-of-sight of the projection. In principle, these areal densities could provide sufficient information to detect the presence or absence of explosives. For example, if no nitrogen is detected in the projection, then there is no nitrogen-based explosive present. In practice, the overlapping of the elemental distributions from spatially separated objects will produce a significant number of false positives (indication of an explosive when not present) and false negatives (failure to detect an explosive when present).

We are developing algorithms in three areas to reduce the number of these false positives and false negatives. In the first area, we use tomographic reconstruction techniques to provide separation of the objects.[6] In reconstruction for medical applications, the goal is to provide an accurate visual image. In our case, the goal is more limited and consists of providing sufficient spatial separation between objects to decrease the number of false positives and false negatives. This more limited objective allows us to relax the demands on the reconstruction accuracy by limiting the number of projections and by using relatively coarse projection resolution. This is fortunate since system requirements will dictate limits on the number of projections and pixel resolution.

In our initial investigations we have kept the number of projections to 5 or fewer and limited pixel resolution to 0.5 to 2 cm. Most of the MCNP modeling was done with a 2-cm resolution. We have used the algebraic reconstruction technique of maximum likelihood with 25 iterations for most of our studies. Initial surveys found that the reconstruction technique and the number of iterations did not have a significant impact on the final results. This could change as we optimize various parameters and include realistic noise distributions.

The second area of investigation involves the development of better signatures for contraband materials. Here the term "signature" is used to represent some combination of the measured elemental densities that indicates the presence of a contraband material. The measured data from a pixel will consist of elemental densities that are due to various contributions of contraband and benign materials. Some of this material will actually be located within the pixel of interest and some will be due to artifacts from the tomographic reconstruction process. There will also be statistical uncertainties in the elemental data due to the finite number of counts detected and to the unfolding process. The goal in this second area is to develop a contraband signature that maximizes the differences between contraband and benign materials given the measured uncertainties. The development of this contraband signature is complicated because the functional relationships between measured elemental densities do not have to be linear, contraband materials of interest often have a wide range of densities and compositions, and benign materials of interest cover a wide range of materials and densities that are not well characterized. An example of this is in detection of explosives in luggage. In this case there is a wide range of explosive densities and compositions as well as a large number of benign objects that are not well characterized in terms of compositions.

Table 1. Selected results of element unfolding for various simulation conditions (number of histories, time resolution, and energy range).

material	element	exact	$1.4 \cdot 10^6$, 2 ns, 0.5-10 MeV	$1.4 \cdot 10^6$, 2 ns, 1-5 MeV	$1.4 \cdot 10^6$, 1 ns, 1-5 MeV
RDX	H	0.0882	0.0778 ± 0.0082	0.0888 ± 0.0111	0.0765 ± 0.0115
	C	0.0441	0.0440 ± 0.0076	0.0442 ± 0.0096	0.0393 ± 0.0100
	N	0.0882	0.0935 ± 0.0078	0.0881 ± 0.0091	0.0953 ± 0.0095
	O	0.0882	0.0897 ± 0.0029	0.0881 ± 0.0041	0.0926 ± 0.0041
PETN	H	0.0804	0.0713 ± 0.0081	0.0859 ± 0.0112	0.0693 ± 0.0114
	C	0.0503	0.0503 ± 0.0076	0.0516 ± 0.0096	0.0451 ± 0.0099
	N	0.0402	0.0452 ± 0.0078	0.0438 ± 0.0091	0.0463 ± 0.0093
	O	0.1207	0.1219 ± 0.0030	0.1216 ± 0.0041	0.1253 ± 0.0041

In our initial evaluation of tomographic reconstruction techniques, we have used a relatively simple contraband signature, which we refer to as the equivalent contraband density signature. Consider a single contraband material. For each pixel an equivalent contraband density is calculated for each measured element by dividing the measured elemental density by the mass fraction of that element in the contraband material of interest. If the pixel contains only contraband material, then each element will yield the same equivalent contraband density to within statistical uncertainties. However, if there is a mixture of other materials, then these values will differ, and the maximum contraband material that can be present in the pixel will correspond to the smallest calculated density. If more than one contraband material is of interest, we calculate the equivalent contraband density for each material of interest and then use the largest equivalent density. For explosives we used a list of 8 different explosives (PETN, RDX, C4, TNT, Nitromethane, Tetryl, TATB, and DATB). For drugs we used cocaine hydrochloride and heroin. The main advantage of this equivalent contraband density signature is the fact that the derived density will always be greater than or equal to the actual contraband density present in that material. The disadvantage is that many benign materials will yield a nonzero contraband density signature and, therefore, lead to an increase in the number of false positives or false negatives.

The third area in which we are exploring different algorithms is image processing. The tomographic reconstruction, combined with a particular contraband signature, provides a two-dimensional density image of a slice of the interrogated object. In this image, pixels with large values are more likely to contain contraband than those with small values. The object is to develop algorithms that will automatically process this image and predict the presence or absence of a contraband object. This process of determining the presence or absence of a particular object within an image is an active area of research in the field of image processing. For these initial studies, however, we divide the equivalent contraband density into four regions, set all pixels within a particular region to the same density, and visually inspect the resulting image. We also determine the amount of contraband material within each region and compare it to the amount actually present.

Figure 5 shows the 3 and 5 angle reconstructions of the bulk explosive phantom of Fig. 2. The upper two images correspond to the equivalent explosive signature (EX) and the corresponding discrete image (EB) for three projections. The bottom two images show the results for 5 projections. The box size is 40 cm and the pixel resolution is 2 cm. The reconstruction used elemental areal densities obtained from unfolding the MCNP transmission data. The presence of the square RDX explosive is clearly seen in all four images. These results indicate that, for bulk explosives with densities similar to that of RDX, a luggage inspection system could be designed with a 2-cm resolution and only three projection angles. It also indicates that the statistical uncertainties due to transmission through the phantom and the elemental unfolding do not significantly distort the final image. As the thickness or density of the explosive decreases the equivalent explosive density will also decrease, making it more difficult to separate the explosive from the surrounding background. This can be offset by increasing the pixel resolution, by increasing the number of projection angles, or by developing improved explosive signatures. We are in the process of investigating some of these questions for thin explosives.

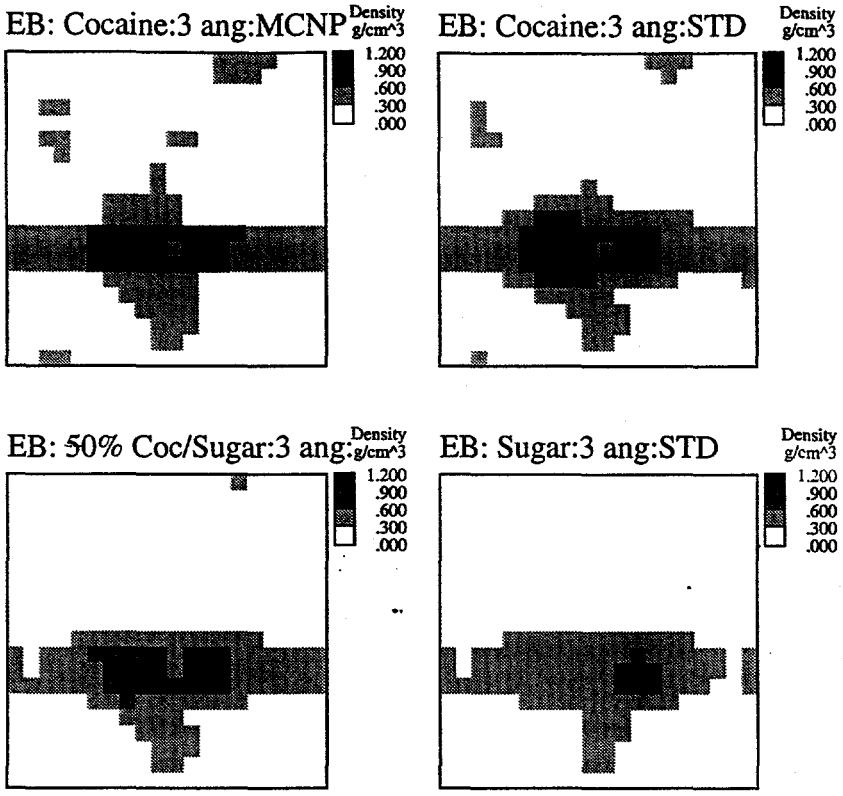

Figure 7. Reconstructed images of a cocaine/sugar phantom.

basis of comparison, Argonne's Tandem Dynamitron at the Fast Neutron Generator facility (now decommissioned) routinely ran with average currents of several microamperes and the pulse structure indicated in footnote (d) to Table 2.

2.3.2 Variation in sample position

Another important parameter for the design of an FNTS system is the relative positions of the neutron source, the sample, and the detector(s). This determines both the footprint and the detector array size of the "spectroscope" portion of the system and impacts on the accuracy of the elemental areal densities which the system determines. The footprint and array

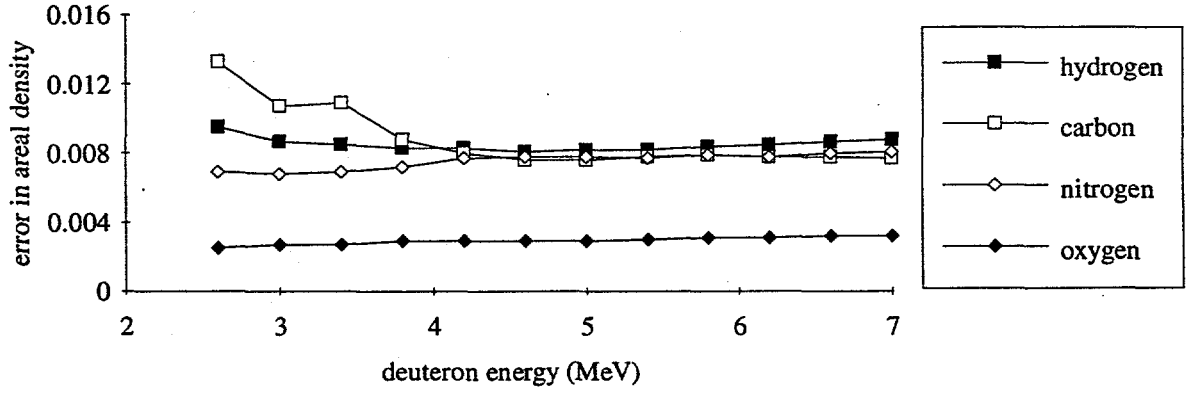

Figure 8. Variation in errors in areal density of H, C, N, and O versus incident deuteron energy for ^{9}Be(d,n) source.

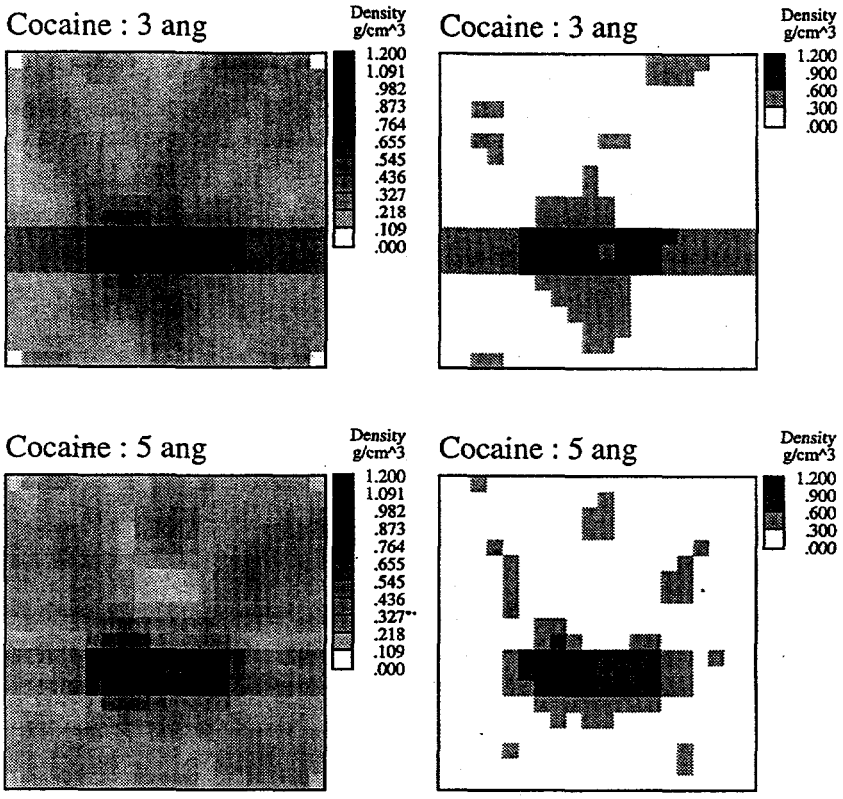

Figure 6. Reconstructed images of a cocaine phantom.

system. We discuss here our efforts to investigate two issues: the accelerator energy required and the relative positions of the neutron source, the detector(s), and interrogated sample.

2.3.1 Variation in incident deuteron energy

We have simulated neutron transmission through a 3-cm sample of RDX explosive using the zero-degree neutron source spectrum from the ^{9}Be(d,n) reaction for 2.6 MeV $\leq E_d \leq$ 7.0 MeV. The uncertainties in the elemental densities of hydrogen, carbon, nitrogen, and oxygen are shown as functions of incident deuteron energy in Figure 8. These results show that there is little dependence of the errors on incident deuteron energy for $E_d \geq 4.0$ MeV, but that the error in carbon increases rapidly for deuteron energies below that level. The reason for this is that there is a kinematic edge in the neutron source spectrum about 1 MeV lower than the deuteron energy (see Fig. 9). Thus for deuteron energies less that 4.2 MeV, the kinematic edge in the neutron source spectrum passes beneath about 3.2 MeV, which is where a significant feature lies in the carbon total cross section (Fig. 9). Likewise, when the deuteron energy is further decreased beneath 3 MeV, the kinematic edge passes beneath 2 MeV, near which lies another resonant feature. Since there are then many fewer neutrons to sample these parts of the energy spectrum, the error in determining the carbon areal density is greater. If carbon detection is important to the detection of explosives, we may be limited to a minimum deuteron energy of about 4 MeV.

The advantage of using a lower deuteron energy is that the accelerator can be of lower energy, and thus smaller. However, in order to detect the same number of neutrons, the accelerator current would have to be higher, since the neutron yield is lower at lower deuteron energies and since the transmission will be lower for the softer source spectrum. The average current required for a detection rate of 10^5 neutrons per second is given in Table 2. The principal advantage of using higher deuteron energy is thus not to have lower elemental uncertainties but lower accelerator current. While a lower deuteron energy is desirable from the point of view of cost and size, we may find that the need for a greater neutron yield may drive us to consider higher deuteron energies because the current required for lower energies may not be available. As a

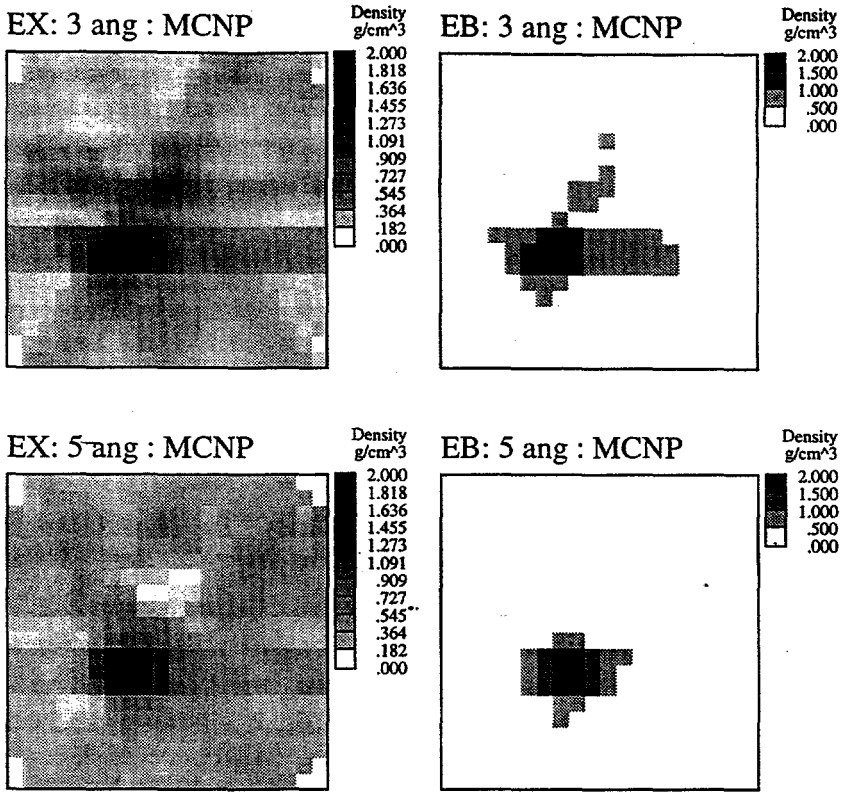

Figure 5. Reconstructed images of the explosive phantom described in Fig. 2.

The same methods used in explosive detection can be applied to the detection of drugs. The cocaine image of Fig. 6 is calculated in the same way as Fig. 5, but with the RDX block of explosive in Fig. 2 replaced by cocaine, the nylon block by paper, the ethyl alcohol cylinder by water, and the silk background by a cotton background. In calculating the equivalent cocaine signature, we did not include the small nitrogen component found in cocaine because the unfolded nitrogen areal density would be zero within statistics. Thus the equivalent cocaine density is based only on H, C, and O. The cocaine is clearly detected in each of these images. The fact that the image of the book is partially detected, however, shows that the equivalent cocaine density is not as good a signature for narcotics as the equivalent explosive density is for explosives This is due to the components and density of paper being similar to that of cocaine. This suggests the need for a better cocaine signature, such as the combination of the equivalent cocaine density with the carbon-to-oxygen ratio used in PFNA.

We have also looked at mixing various materials with the contraband materials. Figure 7 shows several reconstructed images of mixtures of cocaine and sugar using three projections. The upper left image in Fig. 7 corresponds to the reconstructed MCNP image from Fig. 6. The upper right image corresponds to the reconstructed cocaine image using the exact areal projection densities. Exact in this case refers to using the actual two-dimensional elemental densities with no errors introduced. The bottom left image corresponds to a 50% mixture of cocaine and sugar and the bottom right image shows pure sugar. Comparison of the upper two images shows that the statistical uncertainties are not a major factor in the reconstruction process. At the lowest thresholds there is not much difference between the cocaine, 50% mixture, and the pure sugar. However, the images with higher thresholds clearly show that the cocaine and the 50% mixture could be distinguished from that of sugar.

2.3 Systems studies

The design of any interrogation system depends on a number of factors such as size, cost, accuracy, and throughput. We have addressed these issues by modeling a series of simple problems to learn more about the characteristics of an FNTS

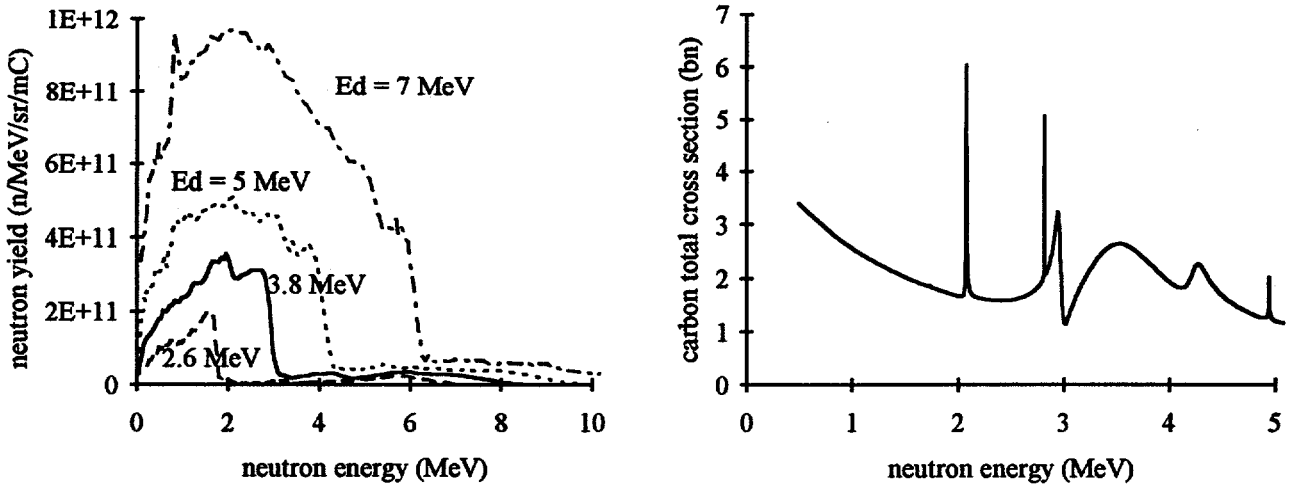

Figure 9. Neutron yield and energy spectrum for the ^{9}Be(d,n) source for various values of incident deuteron energy (left). Total cross section for carbon as a function of neutron energy (right).

Table 2. Deuteron current required for a neutron count rate of 10^5/s as a function of deuteron energy (for the standard TOF geometry, average detector efficiency = 0.15, and a 3-cm RDX sample).

E_d (MeV)	Y_n (n/sr -μC)[a]	transmission[b]	$\langle I_d \rangle$ (μA)[c]	I_p (mA)[d]
2.6	$2.62 \cdot 10^8$	0.421	19.2	9.6
3.0	$4.35 \cdot 10^8$	0.439	11.1	5.6
3.4	$6.41 \cdot 10^8$	0.461	7.18	3.6
3.8	$8.83 \cdot 10^8$	0.479	5.02	2.5
4.2	$1.17 \cdot 10^9$	0.484	3.76	1.9
4.6	$1.50 \cdot 10^9$	0.485	2.93	1.5
5.0	$1.87 \cdot 10^9$	0.485	2.34	1.2
5.4	$2.31 \cdot 10^9$	0.487	1.89	0.95
5.8	$2.80 \cdot 10^9$	0.493	1.54	0.77
6.2	$3.35 \cdot 10^9$	0.500	1.27	0.63
6.6	$3.97 \cdot 10^9$	0.505	1.06	0.53
7.0	$4.66 \cdot 10^9$	0.508	0.90	0.45

[a] Neutron yield data from Ref. 7.
[b] Over the energy range 0.5 - 10 MeV
[c] Average deuteron current
[d] Peak deuteron current (2 ns pulse at 10^6 repetition rate)

size impact on the systems' cost, and the accuracy of elemental unfolding directly impacts the accuracy of the system. Here we examine the effect of changing one parameter, the position of the sample, when the distance between source and detector(s) is kept fixed.

Simulations were run for a 3-cm thick sample of RDX located in a series of positions between the source and detector, every 50 cm from 200 cm to 500 cm (immediately in front of the detectors). The transmission spectrum was unfolded using the transmission-derived cross section sets which are used for unfolding spectra at the standard sample position of 250 cm. The results of these runs are shown in Figure 10. Transmission spectra are shown in an uncollimated detector for sample positions z = 250, 400, 450, and 500 cm. (The spectra for z = 200, 300, and 350 cm are indistinguishable from that for z = 250 cm, and are not shown.) One can see that as the sample is moved closer to the detector, the number of detected neutrons increases. This increased transmission is due to neutrons which have scattered in the sample by only a small angle, but still

hit the detector. Since the value of the cross sections is fixed, a larger number of neutrons counted is interpreted by the unfolding algorithm as being due to a smaller amount of material in the sample. [This is a straightforward result of the basic equation for exponential attenuation, $T = \exp(-n\sigma x)$.] The unfolded elemental densities are shown on the right side of Figure 10 as functions of sample position. The correct elemental abundances can be unfolded up until z = 400 cm, after which the number of scattered neutrons is too great to permit accurate unfolding.

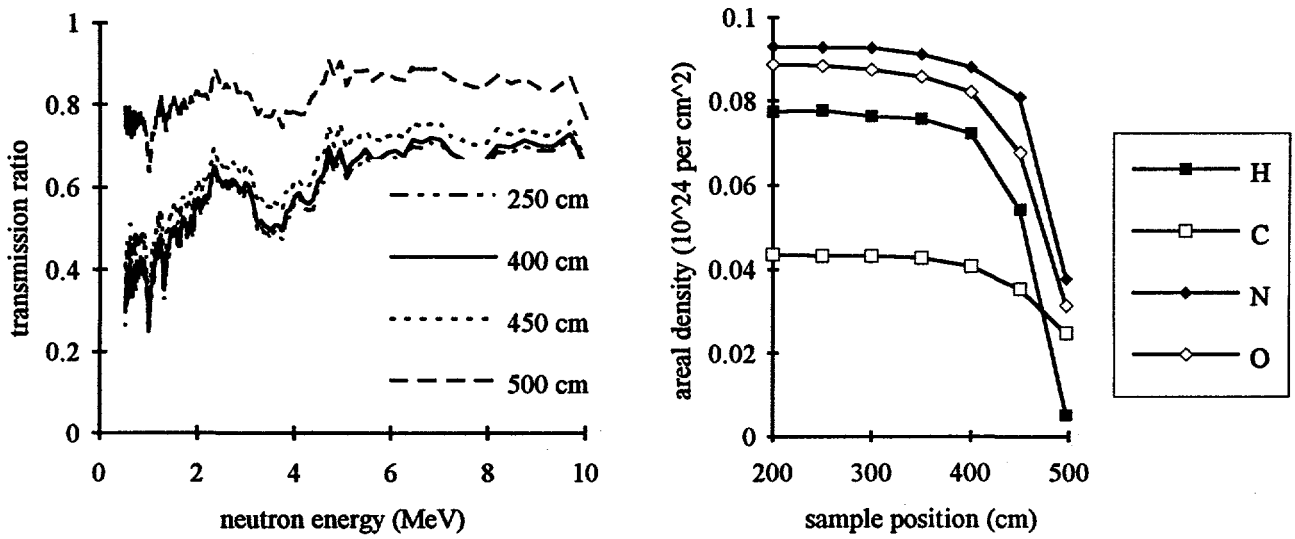

Figure 10. Transmission ratios (left) and unfolded elemental areal densities (right) for a 3-cm thick RDX sample as a function of sample position.

To attempt to improve the unfolded results for z = 500 cm, we constructed a special cross section library for samples located immediately in front of an uncollimated detector. The results showed that the areal elemental densities could not be unfolded correctly. One problem is that the cross sections to be used in unfolding depend quite sensitively on the size and density of the sample, so that it is not possible to create one cross section library which could be used for all sample thicknesses. In all cases, hydrogen is fit poorly for samples in front of the detector. The algorithm uses the various elemental cross sections to match the peaks and valleys in the transmission spectrum. If the overall normalization is incorrect, the algorithm will use smooth cross sections (i.e., hydrogen) to adjust the overall normalization.

3. PULSED FAST-NEUTRON ANALYSIS

Pulsed Fast-Neutron Analysis uses nsec pulses of monoenergetic neutrons produced by accelerating deuterons onto a deuterium gas target. The neutron beam is scanned vertically across the cargo container by a movable collimator. Scanning along the length of the container is accomplished by moving the container horizontally. Depth information is obtained using time-of-flight between the accelerator pulse and the arrival of a gamma ray in NaI detectors located outside the container. Since the neutrons produced have velocities of about 4 cm/ns, the accelerator pulse must be at most a few ns if the voxel depth (thickness) is to be about 10 cm. In luggage or smaller containers, where higher resolution may be required for explosives detection, the minimum pixel dimension along the beam is about 5 cm, since the practical minimum pulse width is about 1.25 ns. The 4.44-MeV gamma from the first excited state in ^{12}C and the 6.13-MeV gamma ray from the second excited state in ^{16}O are used to generate a qualifier that indicates the presence of narcotics. Nitrogen gamma rays can be measured to provide an indication of nitrogen density and thus the presence of explosives.

The gamma-ray signal detected depends sensitively on the incident neutron energy used, since the inelastic scattering cross sections are strong functions of energy. Neutron energies greater than 6.5 MeV are required to detect ^{16}O, with the inelastic scattering cross sections being largest between 8.2 and 8.25 MeV (requiring a deuteron energy of about 5.5 MeV). However, since the inelastic scattering cross sections vary rapidly in this energy range, the energy distribution of the source neutrons must be well-known and stable so that the effective or spectrum-averaged cross sections remain constant.

The PFNA geometry shown in Figure 11 below was modeled with MCNP to estimate the signal at various detector locations for an incident neutron energy of 8.5 MeV. This geometry consisted of a uniform container loading of 0.5 g/cm^3 of sugar ($C_6H_{12}O_6$) with a 25-cm radius sphere of cocaine hydrochloride ($C_{17}H_{21}NO_4HCl$) centered 75 cm from the front face. The same geometry was then modeled with only the background material for comparison. The gamma rays detected per source neutron at a detector in the top center of the container are shown in Figure 12. Examination of the two curves indicates that at a position of about z = 50 cm, there is an increase in the carbon atom density, and perhaps a decrease in the oxygen atom density. Also, the total mass density increases, since the gamma-ray generation rate falls off more quickly with distance into the container.

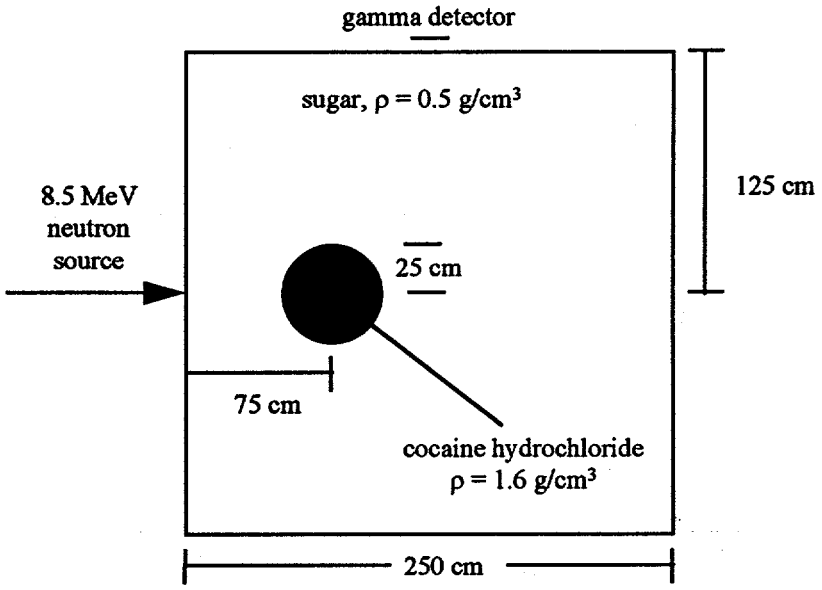

Figure 11. Geometry used for MCNP calculation of PFNA gamma-ray signals.

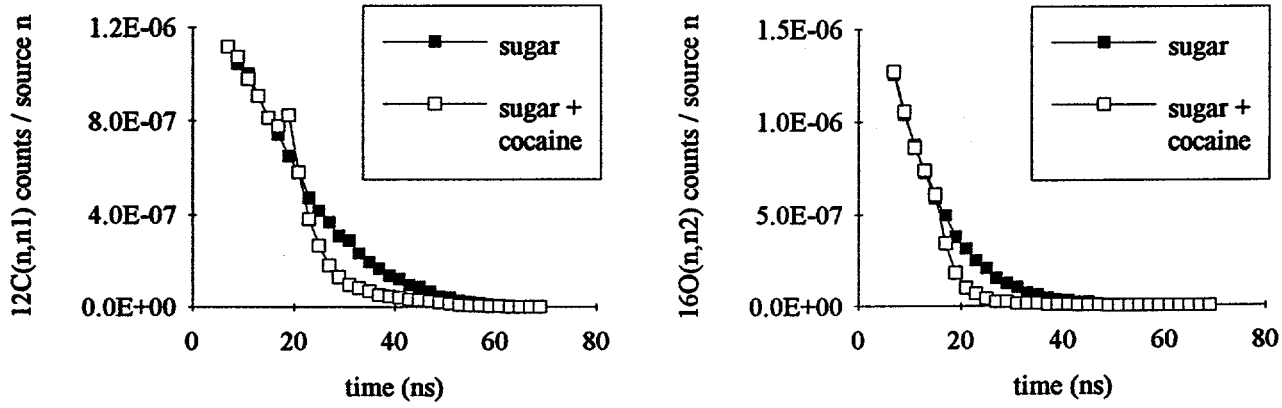

Figure 12. MCNP signal estimates for $^{12}C(n,n1)$ and $^{16}O(n,n2)$ gamma rays for a sugar assembly containing a bulk cocaine sample.

- The gamma-ray signal as a function of time at a certain detector location must then be transformed into information about elemental densities inside the container as a function of position using equations of the type

$$n_c(t_i) = S_c(t_i) / \left[e^{-\lambda z_i} (V\sigma_c) \left(A_d / 4\pi r_i^2 \right) e^{-\mu_c r_i} \right] \quad \text{and} \quad n_o(t_i) = S_o(t_i) / \left[e^{-\lambda z_i} (V\sigma_o) \left(A_d / 4\pi r_i^2 \right) e^{-\mu_o r_i} \right] \tag{1}$$

which correspond to a phenomenological model of gamma-ray generation and transport described in Ref. 8. This model makes the simplifying assumption that gamma rays caused by scattered neutrons are unimportant. To determine n_c and n_o we would have to know the details of the container contents, because we need to know λ, μ_c and μ_o. (where λ is the fast-neutron attenuation constant and μ_c and μ_o are the attenuation coefficients for the carbon and oxygen gamma rays, respectively) as functions of position throughout the container. However, instead of determining densities directly, one might detect cocaine based on the ratio of concentrations C/O. The ratio n_c/n_o can be written as

$$\frac{n_c}{n_o} = \frac{S_c(t_i) \cdot \sigma_o}{S_o(t_i) \cdot \sigma_c} \cdot e^{(\mu_c - \mu_o) r_i}. \tag{2}$$

If the details of the cargo loading are not known ,one can ignore the difference in attenuation between the carbon and oxygen gamma rays, but this will lead to a larger uncertainty in the resulting C/O ratio.

4. CONCLUDING REMARKS

Analytic and Monte-Carlo modeling have proven to be very effective in investigating the system parameters required for luggage and cargo inspection systems. For FNTS, modeling has provided information into the proper accelerator energy, sample positions, flight path length, and time (energy) resolution needed. Tomographic reconstruction with few views and relatively poor resolution shows promise for detecting bulk explosives and narcotics. Detection of thin samples will be more difficult, and is currently being investigated. For PFNA, modeling has given indications of the expected signal strengths in heavily loaded containers. The information provided by our modeling and reconstruction studies can be used to study system design issues and to explore the range of capabilities of the two techniques.

5. ACKNOWLEDGMENTS

This work was sponsored by the U. S. Federal Aviation Administration Technical Center under contract DTFA03-03-X-00021 and by the Office of National Drug Control Policy, Counterdrug Technology Assessment Center under contract 6-CO-160-00-195.

6. REFERENCES

1. J. C. Overley, "Determination of H, C, N, O, Content of Bulk Materials from Neutron-Attenuation Measurements," *J. Appl. Radiat. Isot.* **36**, 185-191 (1985); "Element-Sensitive Computed Tomography with Fast Neutrons," *Nucl. Instr. Meth. Phys. Res.* **B24/25**, 1058-1062 (1987).
2. Z. P. Zawa and T. Gozani, "PFNA Technique for the Detection of Explosives," *Proc. 1st Int'l Symp. on Explosive Detection Technology*, DOT/FAA/CT-92/11, 82-103, Atlantic City, NJ (May 1992); D. R. Brown, R Loveman, J. Bendahan, M. Schulze, "Cargo Inspection System Based on Pulsed Fast-Neutron Analysis," *Proc. Int'l Symp. on Contraband And Cargo Inspection Technology*, 235-241, Washington, DC (Oct. 1992)..
3. B. J. Micklich, M. K. Harper, A. H. Novick, and D. L. Smith, "Illicit Substance Detection Using Fast-Neutron Transmission Spectroscopy," *Nucl. Instr. Meth. Phys. Res.* **A353**, 646-649 (1994).
4. J. Briesemeister, ed., "MCNP - A Generalized Monte Carlo Code for Neutron and Photon Transport, Version 3A," LA-7396-M, Rev. 2, Los Alamos National Laboratory (Sept. 1986).
5. E. J. Burge, "Errors and Mistakes in the Traditional Optimum Design of Experiments on Exponential Absorption," *Nucl. Instr. Meth.* **144**, 547-555 (1977).
6. C. L. Fink, B. J. Micklich, T. J. Yule, P. Humm, L. Sagalovsky, and M. M. Martin, "Evaluation of Neutron Techniques for Illicit Substance Detection," to be published in *Nucl. Instr. Meth.*
7. J. W. Meadows, "The Thick-Target ^{9}Be(d,n) Neutron Spectra for Deuteron Energies Between 2.6 and 7.0 MeV," ANL/NDM-124 (Nov. 1991); *Nucl Instr. Meth. Phys. Res.* **A324**, 239-246 (1993).
8. B. J. Micklich, C. L. Fink, and T. J. Yule, "Key Research Issues in the Pulsed Fast-Neutron Analysis Technique for Cargo Inspection", SPIE **2276**, 310-320, San Diego, CA (1994).